journal

J. Am. Ceram. Soc., **89** [12] 3599–3609 (2006)
DOI: 10.1111/j.1551-2916.2006.01382.x

Direct Ink Writing of Three-Dimensional Ceramic Structures

Jennifer A. Lewis[†]

Materials Science and Engineering Department, Frederick Seitz Materials Research Laboratory, University of Illinois at Urbana-Champaign, Urbana, Illinois 61801

James E. Smay

Chemical Engineering Department, Oklahoma State University, Stillwater, Oklahoma 74078

John Stuecker and Joseph Cesarano III

Sandia National Laboratories, Albuquerque, New Mexico 87185

The ability to pattern ceramic materials in three dimensions (3D) is critical for structural, functional, and biomedical applications. One facile approach is direct ink writing (DIW), in which 3D structures are built layer-by-layer through the deposition of colloidal- or polymer-based inks. This approach allows one to design and rapidly fabricate ceramic materials in complex 3D shapes without the need for expensive tooling, dies, or lithographic masks. In this feature article, we present both droplet- and filament-based DIW techniques. We focus on the various ink designs and their corresponding rheological behavior, ink deposition mechanics, potential shapes and the toolpaths required, and representative examples of 3D ceramic structures assembled by each technique. The opportunities and challenges associated with DIW are also highlighted.

I. Introduction

New methods for materials fabrication at the micro- and nano-scale will drive scientific and technological advances in areas of materials science, biology, chemistry, and physics.[1,2] The broad diversity of potentially relevant materials, length scales, and architectures underscores the need for flexible patterning approaches. Three-dimensional (3D) structures fabricated from colloidal "building blocks" may find widespread technological application as advanced ceramics,[1–3] sensors,[4–7] composites,[8–11] tissue engineering scaffolds,[12–14] and photonic[15–17] materials. Many of these applications require architectures that are engineered at length scales far exceeding colloidal dimensions with lattice constant(s) ranging from several micrometers to millimeters. Direct ink writing (DIW) techniques[2,18] offer a powerful route for producing complex 3D structures, including space-filling solids and structures with high aspect ratio walls or spanning (unsupported) elements.

The term "direct-write assembly" broadly describes fabrication methods that use a computer-controlled translation stage, which moves a pattern-generating device, e.g., ink deposition nozzle or laser writing optics, to create materials with controlled architecture and composition.[2,18] Several direct ink writing techniques have been introduced that are capable of patterning materials in 3D, including 3D printing (3DP),[19–21] direct ink-jet printing,[22–24] hot-melt printing,[25–28] robocasting,[29–35] fused deposition,[4,5,36,37] and micropen writing[38] (see Table I). We divide DIW into *droplet-* and *filament-based* approaches and prominently feature four of these techniques, as shown schematically in Fig. 1.

Our feature article on direct ink writing of 3D ceramics structures is organized as follows: in Section II, we provide a brief overview of the basic design principles associated with computer-aided manufacturing. The success of DIW techniques hinges critically on the creation of an informed component design that accounts for the capabilities and limitations of the specific technique utilized. Sections III and IV describe representative ink formulations and their corresponding rheological behavior, ink delivery mechanics, and assembly strategies used by droplet- and filament-based DIW techniques, respectively, within the context of fabricating 3D ceramic structures. Several examples of DIW-derived structures are highlighted in each section, and, where possible, we present components of similar design and composition to facilitate direct comparison. Finally, we offer a perspective on the future opportunities and challenges for this approach in Section V.

D. Green—contributing editor

Manuscript No. 22224. Received September 8, 2006; approved October 2, 2006.

This material is based on work currently supported by the National Science Foundation (Grant# DMR01-17792), U.S. Department of Energy, through the Frederick Seitz Materials Research Laboratory (Grant# DEFG02-91ER45439), the Army Research Office (Award# DAAD19-03-1-0227), the Air Force Office of Scientific Research (Award# FA9550-05-1-0092, Subaward# E-18-C45-G1), and Sandia National Laboratories. Sandia is a multiprogram laboratory operated by Sandia Corporation, a Lockheed Martin Company, for the United States Department of Energy's National Nuclear Security Administration under contract DOE-AC04-94AL85000.

[†]Author to whom correspondence should be addressed. e-mail: jalewis@uiuc.edu

Feature

Table I. Droplet- and Filament-Based Techniques for DIW

	Ink design	Minimum printed feature size	References
Droplet-based DIW			
3D Printing	Binder solution printed on powder bed	170 μm lateral 45 μm depth	Moon *et al.*[20]
Ink-jet Printing	Colloidal fluid	20 μm lateral 100 nm height	Zhao and colleagues[22,39,40]
Hot-melt ink-jet printing	Colloid-filled wax (max solids ~40%)	70 μm lateral <1 μm height	Reis and colleagues[25,26,27,28]
Filament-based DIW			
Robocasting (in air)	Concentrated colloidal gel	500 μm diameter	Cesarano and colleagues[29,30,31,32,41,42]
Robocasting (in oil)	Concentrated colloidal gel	200 μm diameter	Smay *et al.*[6,33,34]
	Concentrated nanoparticle gel	30 μm diameter	Li and Lewis[43]
Fused deposition	Particle-filled polymer melt (max solids ~50%)	100 μm diameter	Allahverdi and colleagues[4,5,36,44,45]
Micropen writing	Concentrated colloidal fluid	25 μm diameter	Morissette *et al.*[38]

DIW, Direct ink writing; 3-D, three-dimension.

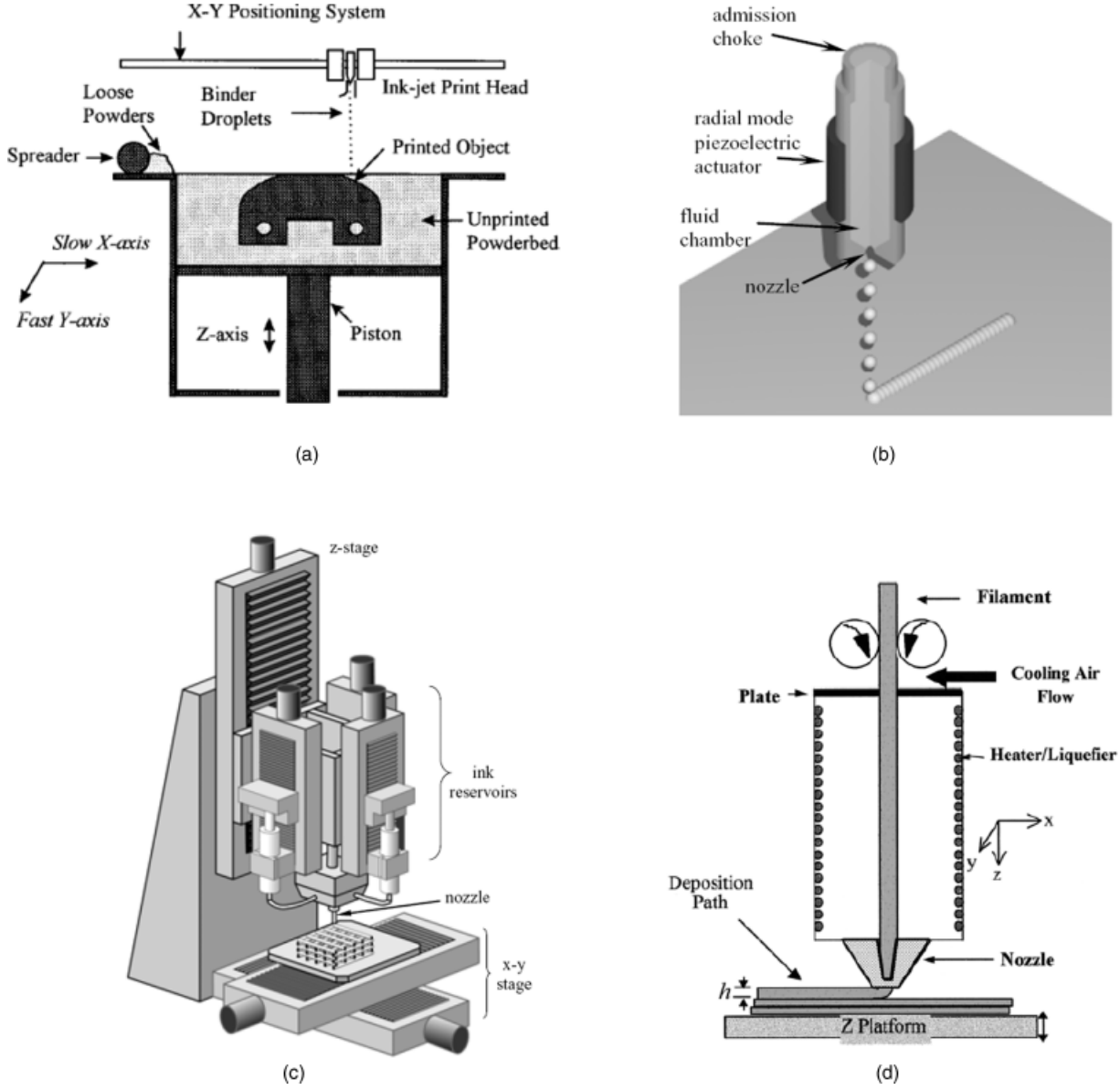

Fig. 1. Schematic illustrations of both droplet- and filament-based direct ink writing techniques: (a) three-dimensional printing (3DP™),[20] (b) direct ink-jet printing (DIJP),[22] (c) robocasting,[34] and (d) fused deposition of ceramics.[4]

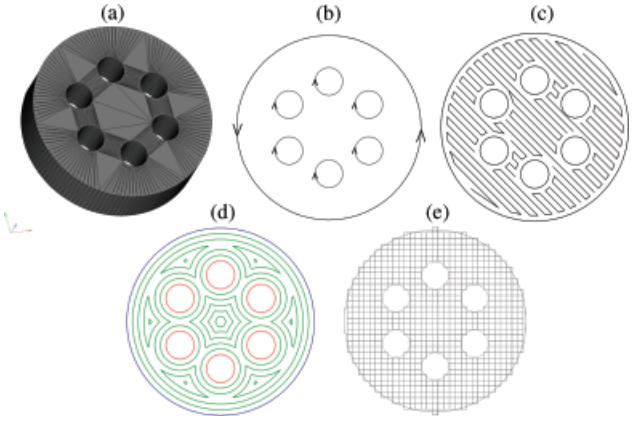

Fig. 2. (a) Stereolithography (.stl) model of a simple disk with vias, (b) positive and negative loops from a representative slice, (c) raster fill tool path, (d) contour fill tool path, (e) pixel fill pattern.

II. Design Principles

DIW techniques must produce ceramic structures within acceptable geometric tolerance having properties comparable with or superior to that achievable by traditional fabrication routes. The properties of interest may include strength, electrical properties, chemical activity, biological function, or esthetic features. In its simplest form, DIW can be used as a rapid prototyping tool for designs that will be produced by traditional means. However, DIW also offers the potential to create 3D ceramic structures with locally varying structure, composition, and properties that cannot otherwise be fabricated. Like other layered manufacturing techniques, the design process starts with the creation of a computer model of the component to be assembled. Figure 2(a) illustrates a rendered stereolithography (.stl)[46] file for a simple disk with six vias. The .stl format defines the surface of a 3D object with a mesh of vertex and edge-sharing facets with outward-pointing normal vectors. Next, the .stl model is sliced by a series of parallel planes with fixed interplane spacing equivalent to the thickness of the layers that will be printed. Figure 2(b) illustrates the positive (counterclockwise loop) and negative (clockwise loops) areas associated with a representative layer (slice). During DIW, the positive areas are filled with ink, while the negative areas are not. Differences between droplet and filament printing mechanics necessitate a divergence in strategy for infilling these areas, as described in subsequent sections.

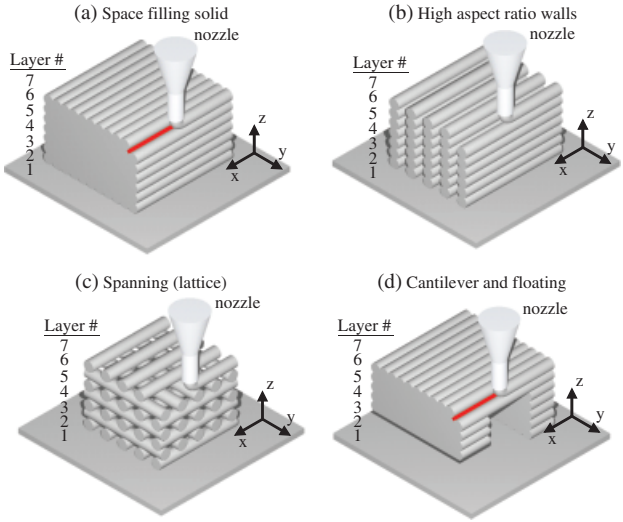

Fig. 3. Possible structural features encountered in direct-write assembly, illustrated for filament-based writing: (a) solid space filling, (b) high aspect ratio walls, (c) spanning (or lattice), (d) cantilevered and floating structures.

After slicing and calculation of tool paths for each layer, the 3D object is examined to identify whether support structures are needed. Figure 3 shows the four basic patterns encountered in DIW. For space-filling solids, the deposited ink must flow to form a continuous body without "knit lines" in or between layers. For high aspect ratio walls and spanning structures, the tool-path spacing within individual layers must exceed the deposited droplet or filament width. In the case of spanning structures, gaps in underlying layers must be bridged by overlying layers. The final case is cantilevered and floating elements, in which portions of layers are either completely unsupported (floating) or attached to underlying layers in a cantilevered fashion. The DIW design process therefore requires: (1) the ability to assemble the four basic structures described above, (2) control over the lateral ($x-y$) and vertical (z) spacing of the tool path (i.e., resolution), (3) compositional control within the tool path, (4) control over the rate of ink deposition, and (5) proper accounting for the dimensional and property changes that occur during post-deposition processes (i.e., drying, binder removal, and sintering).

III. Droplet-Based Writing

Droplet-based approaches to direct writing of 3D ceramic structures include 3DP,[19–21] direct ink-jet printing,[22–24] and related approaches, such as hot-melt printing.[25–28] Each of these techniques relies on ink-jet printing of material in the form of droplets in a desired pattern via a layer-by-layer build sequence. Ink-jet printing is an established technology with many applications, including reprographic, microdispensing, and materials assembly. Conventional inks for reprographic applications include dye- or pigment-based inks, which are formulated using either a low-viscosity fluid that must be removed by absorption and evaporation or a wax-based system that is heated during droplet formation and then solidified upon impact cooling. These inks serve as models for the ink designs developed for direct-write assembly of ceramics via droplet-based deposition.

(1) Ink Delivery

There are two types of ink delivery systems for droplet-based writing: (1) continuous[23,39] and (2) drop-on-demand[22,25–28,40] ink-jet printing. In either system, the ink is delivered as discrete droplets (see Figs 1(a) and (b)) of fixed volume dispensed from a single or multi-nozzle array. The droplet size depends on the nature of the drop-generating nozzle and on the ink rheology. In continuous-jet printing, ink droplets must be electrically charged upon exiting the nozzle so that the droplet stream can be steered through deflecting electrodes before the ink reaches the substrate.[39] The deflected (or unprinted) droplets must be recovered and recirculated through the ink reservoir. In drop-on-demand printing, ink droplets are produced only when required either by exciting a piezoelectric actuator at a controlled frequency or by locally heating to create pressure pulses in a fluid chamber that cause the ejection of an ink droplet with each pressure cycle. A schematic illustration of a drop-on-demand nozzle is shown in Fig. 1(b). The continuous-jet method allows large areas to be patterned at relatively high speeds, whereas the drop-on-demand method is better suited for depositing small and controlled quantities of material.[20]

The fluid dynamics involved in drop formation and spreading play an important role in the ink design. Reis *et al.*[25] and Seerden *et al.*[28] provide a good overview of these considerations for drop-on-demand printing, whose salient features are summarized here. The behavior of fluid inks during the droplet formation process is dependent upon the Ohnesorge number (Z) given by

$$Z = \frac{\mathrm{We}^{1/2}}{\mathrm{Re}} = \frac{\eta}{(\gamma \rho a)^{1/2}} \tag{1}$$

where We is the Weber number ($= \rho v^2 a/\gamma$), Re is the Reynolds number ($= v a \rho/\eta$), v is the ink velocity, a is a characteristic length (i.e., nozzle diameter), and η, γ, and ρ are the viscosity, surface tension, and density of the ink, respectively. Z expresses the relative importance of viscous, surface tension, and inertial forces for fluid flow. If Z is too high, then viscous forces dominate and a large pressure change is required for droplet ejection. If Z is too low, then unwanted satellite droplets are produced. Successful drop formation (ejection) generally occurs for Z values of 0.1–1.

Drop spreading on impact influences the thickness of the deposited layer and the lateral resolution of materials produced by ink-jet printing. Drop spreading can be estimated by[28]

$$\frac{r_{max}}{r} = \left(\frac{We^2 + 12}{3(1 - \cos\theta) + 4We^2/Re^{1/2}} \right)^{1/2} \quad (2)$$

where r_{max} is the maximum drop radius after impact, r is the initial drop radius, and θ is the contact angle between the ink and the substrate. This expression represents an upper value for r_{max}, because drop spreading is evaluated for a dense substrate in the absence of solidification. In practice, droplet spreading is influenced by the porous nature of the underlying powder bed or printed structure as well as the time required for a given droplet to solidify after deposition.

A final concern for droplet-based DIW is the potential for the impinging droplets to splash on impact with the substrate (or underlying layers). Drop splashing occurs above a critical value of the parameter, K:

$$K = WeRe^{1/4} \quad (3)$$

For example, Seerden *et al.*[28] have reported K_{crit} values of 57.7 for water and methanol, and 102 and 137 for paraffin wax on cold (23°C) and hot (73°C) surfaces, respectively.

The speed with which a component can be assembled using droplet-based writing is a function of the frequency of droplet generation, the dot pitch of the printer, and ink solidification kinetics. Assuming a fixed droplet diameter, the volumetric droplet delivery rate (Q) for single-nozzle scales with its driving frequency (f) is

$$Q = f\frac{4}{3}\pi r^3 \quad (4)$$

where r is the droplet radius. The linear write speed for a space-filling layer is given by

$$v = \frac{Q}{h\Delta y} \quad (5)$$

where h is the layer thickness and Δy is the lateral droplet spacing (i.e., dot pitch). For example, an $f = 5$ kHz jet of $r = 35$ μm droplets with layer and lateral spacings of $h = 18$ μm and $\Delta y = 100$ μm, respectively, result in $Q = 0.9$ μL/s and $v = 0.5$ m/s. This write speed does not account for delays that may be needed due to solidification of previously deposited ink.

(2) Ink Rheology and Solidification

Three ink designs have been utilized to date in droplet-based DIW approaches: (1) binder solutions,[19–21] (2) colloidal fluids,[22–24] and (3) colloid-filled waxes.[25–28] In each case, the inks must be formulated to achieve the desired rheological, drop formation, and solidification behavior during assembly. In 3DP, ceramic structures are formed by spreading powder in a thin layer, followed by selective deposition of binder-based droplets that locally fuse particles together upon drying (see Fig. 1(a)). Moon *et al.*[20] have shown that the infiltration behavior of these droplets into the powder bed depends strongly on polymer molecular weight, and that values less than 15 000 g/mol are required for this approach. Aqueous-based binder solutions are preferred over solvent-based formulations due to their improved jet stability. Finally, they have also shown that the binder concentration (or dose) influences the size of the printed features created by 3DP (see Fig. 4).

Direct ink-jet printing of ceramics from colloidal inks was first demonstrated by Teng *et al.*[24] In this approach, the inks may either be solvent-based[27,40] in which the droplets solidify by drying, or wax-based[22,25–28] in which the droplets solidify by freezing of the wax carrier. For solvent-based systems, stable inks with a colloid volume fraction (ϕ) ranging from 0.025[40] to 0.20[27] have been successfully used. For these inks, particle agglomeration can lead to poor performance of the droplet-producing jet and eventual nozzle clogging. Steric dispersion of the ceramic particles, followed by ultrasonication and sedimentation (or filtration), has been used to remove problematic agglomerates.[40] Dilute inks ($\phi = 0.025$) undergo significant droplet spreading and shrinkage upon drying, leading to printed layers with thin vertical and large lateral dimensions (i.e., approximately 0.4 and 200 μm, respectively).[40] To create structures of substantial thickness (>1 μm), more concentrated colloidal fluids are necessary.[22] De-wetting of the substrate or underlying layers after droplet deposition can occur when the mobile fluid layer persists for appreciable times. To improve print quality, heated air can be made to flow over the structure to enhance

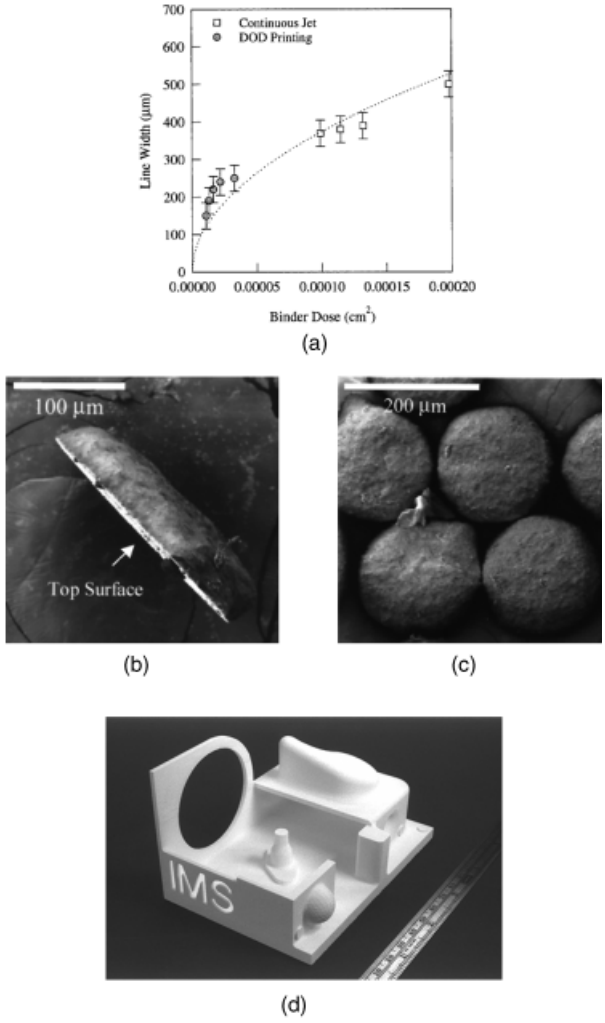

Fig. 4. (a) Line width created by three-dimensional printing (3DP) of a 20 v/o polyacrylic acid binder solution onto a 1 μm powder bed using a continuous jet or drop-on-demand (DOD) printhead. Corresponding (b) side view and (c) bottom view of a single-droplet primitive printed by the latter approach. (d) Optical image of IMS component printed by 3DP ((a)–(c) from Moon *et al.*[20]).

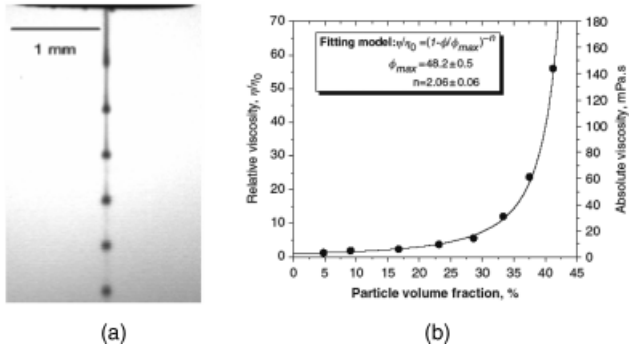

Fig. 5. (a) Stroboscopic image of a concentrated lead zirconate titanate (PZT) suspension (40 vol% solids) being deposited by an ink-jet printhead with a nozzle diameter of 70 μm at a pulse voltage of 70 V, a frequency of 10.5 kHz, a pulse width of 40 μs, and a temperature of 110°C, and (b) suspension viscosity as a function of PZT volume fraction measured at a shear rate of ~100–200 s^{-1} and a temperature of 110°C. The continuous line in (b) is a fit of the data to the Krieger–Dougherty relation (from Wang and Derby[26]).

drying kinetics; however, the dwell times (~20 s) required are considerable, leading to a significant bottleneck in the process.[22,23]

Derby and colleagues[25–28] have recently shown that wax-based inks offer great promise for direct ink-jet printing of ceramics. These inks allow for rapid deposition, good lateral resolution, and high solids loading. In this case, the ink consists of a stable dispersion of ceramic particles in low melting temperature paraffin wax. Inks with a high colloid volume fraction ($\phi \sim 0.40$) have been successfully formulated, which exhibit a good fit to the Krieger–Dougherty relation under suitable printing conditions (e.g., 110°C at shear rates of ~100–200 s^{-1}; see Fig. 5).[28] These molten inks solidify upon deposition by initially cooling at a ring of contact with the underlying substrate, which mitigates further droplet spreading.[28]

(3) Potential Shapes

To create 3D ceramic components of pre-defined shape and dimensions, droplet-based DIW techniques rely on the pixel array approach illustrated in Fig. 2(e). In this scheme, each square in the overlaid mesh is filled by a single droplet. The lateral and vertical resolution within the layer are determined by the droplet size, the extent of droplet spreading upon deposition on the substrate (or underlying layers), and deformation of the droplet upon solidification. The printing rate is limited by the drying or solidification time required for the as-deposited droplets as well as the rate of droplet delivery by the nozzle.

3DP can be used to produce ceramic components with any of the four structural elements shown in Fig. 3, as the unprinted regions of the powder bed provide support to the as-printed features (see, e.g., Fig. 4(d)). In sharp contrast, direct ink-jet printing is incapable of producing structures with spanning, cantilevered, or floating elements without the use of a fugitive support material. Fugitive formulations, such as unfilled wax or water-soluble inks, have been developed, which can be removed during post-processing.[26]

Wang and Derby[26] recently printed solid, pyramidal $Pb(Zr_{0.53}Ti_{0.47})O_3$ structures using a wax support as a buttress. Figures 6(a)–(c) shows the evolution from as-printed to sintered (~99% of theoretical) structures for this functional ceramic component.[26] This work builds on earlier efforts by Seerden *et al.*,[28] in which an alumina-filled ($\phi = 0.30$) wax was printed at 100°C to form 3D structures composed of high aspect ratio walls with a minimum lateral feature size of ~100 μm (see Fig. 6(d)). In this example, the ink viscosity ranged from 7 to 15 mPa · s, the droplet velocity ranged from 5 to 10 m/s, scaling linearly with the amplitude of the pressure pulse, and $Z = 0.365$. Alternatively, Zhao *et al.*[22] demonstrated that similar structures (minimum wall thickness of ~200 μm) could be ink-jet printed under ambient conditions from colloidal fluids ($\phi \sim 0.14$), as shown in Fig. 6(e).

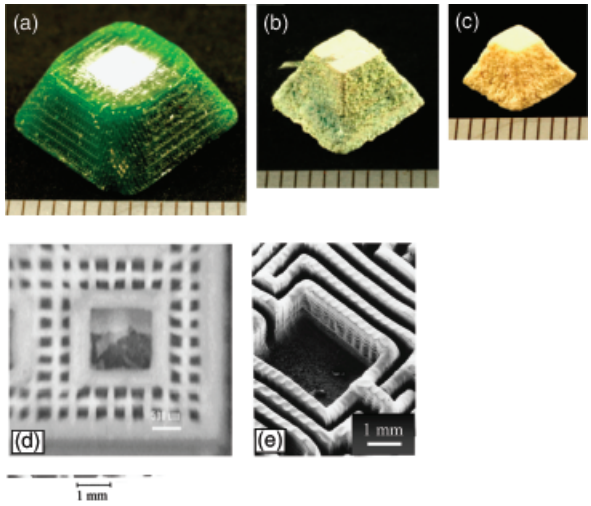

Fig. 6. (a)–(c) Optical image sequence of a ceramic object produced by hot-melt printing of a lead zirconate titanate ink (40 vol% solids) at 110°C, showing (a) the as-printed object with an external wax support, (b) the object after the external support is removed, and (c) the structure after sintering. (Note: Scale divisions are 1 mm.) (d) Optical image of a ceramic object produced by hot-melt printing of an alumina ink (30 vol%) at 100°C, in which the pore channels are connected in only one dimension. (e) Optical image of a ceramic object produced by direct ink-jet printing of a zirconia ink (14 vol% solids). (Images (a)–(c) from Wang and Derby,[26] (d) from Lee and Derby,[28] (e) from Zhao *et al.*[22])

(4) Post-Deposition Processing

The ceramic green bodies produced by droplet-based DIW can be sintered to a high density (i.e., >97% of theoretical).[22,26] For binder solution (3DP) and solvent-based colloidal fluids, the as-dried green body contains sufficient polymeric binder (~2–5 v/o) to facilitate post-deposition handling as well as their rapid removal during heat treatment. In the 3DP process, removal of the printed structure from the powder bed is a necessary step that may result in trapped powder in complex geometries.

For colloid-filled wax-derived structures, the organic content typically exceeds 50% by volume. While this results in high green strength, it also leads to two major problems that arise during binder removal. First, the overall time required to remove the organic phase can be rather lengthy. For example, the samples shown in Figs 4(a)–(c) required 62 h of debinding.[26] Second, these components may experience significant dimensional changes (or slumping) during the debinding process, as both ink and fugitive support liquefy at modest temperatures. To combat dimensional changes, Wang and Derby[26] have packed their structures in carbon black powder to aid in initial wax removal and provide additional structural support.

IV. Filament-Based Writing

Filament-based approaches to direct writing of 3D ceramic structures include robocasting,[29–32,47] fused deposition of ceramics (FDC)[4,5,36,37] and related approaches (i.e., multiphase jet solidification (MJS)[48] and extrusion freeform fabrication (EFF)),[49] and micro-pen writing.[38] In each approach, ink is continuously extruded through a fine cylindrical nozzle (or orifice) to create a filamentary element. Both robocasting and FDC-based approaches are well suited for the assembly of 3D ceramic components, while micro-pen writing is better suited for producing multilayer electroceramic devices on planar and curvilinear substrates.

(1) Ink Delivery

There are two types of ink delivery systems for filament-based writing: (1) constant-displacement and (2) constant-pressure extrusion. In either system, the ink is extruded as a continuous filament through a single or multi-nozzle array. The filament diameter is determined by the nozzle diameter, ink rheology, and printing speed. During constant-displacement printing, ink filaments are extruded at a uniform volumetric flow rate. For example, in robocasting, this is done by mechanically displacing the plunger on the ink reservoir at the pressure required to maintain the desired flow conditions (see Fig. 1(c)). In fused deposition-based approaches, either a colloid-filled polymer filament[4,5,36,37] a or ceramic/binder blend[48,50,51] is extruded at a constant rate through a heated liquefier, where it melts to form a shear thinning, particle-filled organic fluid. The flow rate is controlled by the rate at which the feedstock enters the heated liquefier chamber (see Fig. 1(d)). In constant-pressure writing, ink filaments are extruded by applying a uniform pressure to the reservoir. This approach is less common as slight variations in rheological properties induce fluctuations in the volumetric flow rate.

The ink flows through the deposition nozzle when a pressure gradient ΔP is applied along the length and a radially varying shear stress (τ_r) develops:

$$\tau_r = \frac{r\Delta P}{2l} \tag{6}$$

where r is the radial position within the nozzle (i.e., $r = 0$ at the center axis and $r = R$ at the nozzle wall). Depending upon the velocity profile and the ink stability, plug or laminar flow may occur within the nozzle.[33,52] For example, colloidal gel-based inks consist of a percolating network of attractive particles that are capable of transmitting stress above a critical volume fraction, ϕ_{gel}.[33] When stressed beyond their yield point (τ_y), they exhibit shear thinning flow behavior due to the attrition of particle–particle bonds within the gel, as described by[53]

$$\tau = \tau_y + K\dot{\gamma}^n \tag{7}$$

where τ is the shear stress, n is the shear thinning exponent (<1), K is the viscosity parameter, and $\dot{\gamma}$ is the shear rate. Gel-based inks flow with a three-zone velocity profile within the cylindrical deposition nozzle that consists of an unyielded (gel) core moving at a constant velocity surrounded by a yielded (fluid) shell experiencing laminar flow and a thin slip layer devoid of colloidal particles at the nozzle wall.[52,54] The ink exits the nozzle as a continuous, rod-like filament with a rigid (gel) core-fluid shell architecture, which simultaneously promotes its shape retention while allowing the rods to fuse together at their contact points. The rod architecture is dynamic in nature, such that the fluid shell transforms to the gelled state as particle bonds reform.[55] In contrast, inks that do not possess a yield stress exhibit laminar flow during extrusion.

(2) Ink Rheology and Solidification

Two ink designs are used in filament-based DIW approaches: (1) aqueous colloidal gels[31–34,47,43] and (2) colloid-filled thermoplastic polymers.[4,5,36,37] In each case, the inks must be formulated to achieve the desired rheological, filament formation, and solidification behavior during assembly. In its original conception, robocasting involved the filamentary extrusion of concentrated colloidal gels that were deposited and dried in air.[32] More recently, concentrated colloidal[33] and nanoparticle gels[43] have been extruded into a non-wetting oil bath that suppresses drying and allows finer features to be patterned without clogging the nozzle. Initial shape retention is achieved by the rapid dynamic recovery ($\sim$1 s) of the gel elasticity (i.e., yield stress and modulus) after extrusion,[33,56] followed by removal of the oil and final drying. In fused deposition-based techniques,[5,36] a colloid-filled, polymer melt is extruded at an elevated temperature and solidification occurs upon cooling. This general approach evolved from fused deposition modeling (FDM), in which pure polymeric filaments are used as feedstock.

Cesarano *et al.*[32] pioneered the use of flocculated colloidal suspensions (or gels) as inks for robocasting of ceramics. In their work, filament formation and initial shape retention are achieved by tailoring the ink viscosity, yield strength, and drying kinetics. The inks are formulated close to the maximum solids loading (ca. $\phi_{max} \sim 0.6$–0.64) to minimize drying-induced shrinkage and cracking. With only modest drying, the ink filaments experience a rapid increase in their viscosity, undergoing a transition from pseudoplastic-to-dilatant behavior. Robocasting (in air) is amenable to ink deposition through nozzles with diameters exceeding 500 μm. When depositing structures with finer feature sizes, rapid drying of the ink at the nozzle tip leads to clogging. Robocasting (in air) is suitable for the assembly of relatively large ceramic structures, including those with spanning features. During the build sequence, the ink deposition rate should be synchronized with the drying kinetics to allow for a sufficient increase in yield strength of underlying layers.

Smay and colleagues[6,33,34] have recently demonstrated that colloidal-gel-based inks with a lower colloid volume fraction can be engineered with the appropriate rheological behavior to enable direct writing of 3D ceramic structures. These inks can be patterned within a non-wetting oil bath, thereby decoupling the deposition kinetics from the drying process. Drying-induced nozzle clogging is also suppressed, which enables the creation of 3D ceramic structures with features less than 100 μm.

In either case, robocasting inks need a controlled viscoelastic response, i.e., the colloidal gels must flow through a deposition nozzle and then "set" immediately to facilitate shape retention of the deposited features even if they span gaps in the underlying layer(s). The ink must also fuse to previously deposited material. These characteristics are achieved with careful control of colloidal forces to first generate a highly concentrated, stable dispersion, followed by inducing a system change (e.g., ΔpH, ionic strength, or solvent quality) that promotes the fluid-to-gel transition illustrated schematically in Fig. 7(a). Specifically, the colloid volume fraction (ϕ) of the gel-based inks is held constant, while their elastic properties are tuned by tailoring the strength of the interparticle attractions according to the scaling relationship[57] given by

$$y = k\left(\frac{\phi}{\phi_{gel}} - 1\right)^x \tag{8}$$

where y is the elastic property of interest (shear yield stress (τ_y) or elastic modulus (G')), k is a constant, ϕ_{gel} is the colloid volume fraction at the gel point, and x is the scaling exponent ($\sim$2.5). The equilibrium mechanical properties of a colloidal gel are governed by two parameters: ϕ, which is proportional to the interparticle bond density, and ϕ_{gel}, which scales inversely with bond strength. As the attractive forces between particles strengthen, colloidal gels (of constant ϕ) experience a significant increase in their elastic properties (see Figs 7(b) and (c)). As described by Smay *et al.*,[33] the magnitude of the yield stress and the time required for deposited ink to return fully to its gelled state control the ability of ink to build unsupported spanning structures.

This general approach of creating colloidal gel-based inks can be extended to any type of colloidal or nanoparticulate material, provided their interparticle forces are controlled to produce the desired viscoelastic response. In addition to a simple pH change, the requisite ink rheology may be achieved through the addition of salt[41,43] or oppositely charged polyelectrolyte species,[56,58] as recently demonstrated for nanoparticle and other colloidal inks, respectively. These strategies have been used to produce colloidal inks from a broad array of ceramic materials, including silica,[34] alumina,[32,58] lead zirconate titanate,[6,35] barium titanate,[43,56] mullite,[41] silicon nitride,[59–61] and hydroxyapatite (HA).[13,14]

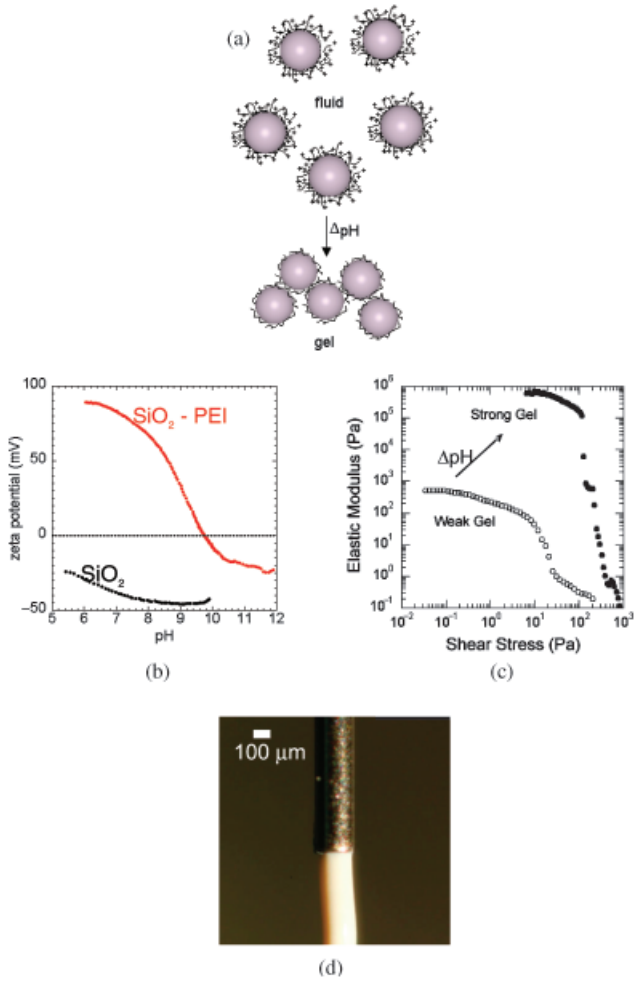

Fig. 7. (a) Schematic illustration of the fluid-to-gel transition observed for colloidal inks, (b) plot of ζ potential versus pH for a dilute suspension of poly(ethylenimine) (PEI)-coated silica (red) and bare silica (black) microspheres in water, (c) corresponding log–log plot of their shear elastic modulus versus shear stress for concentrated silica gels of varying strength: open symbols denote weak gel (pH 9.5) and filled symbols denote strong gel (pH 9.75), and (d) optical image of nanoparticle gel-based ink being extruded through a fine deposition nozzle (diameter of 100 μm). (Note: The point-of-zero charge for PEI-coated silica microspheres occurs at pH 9.75, which is significantly above the value (pH 2–3) observed for bare silica particles. The weak gel had insufficient strength to support its own weight during deposition, whereas the strong gel could be successfully patterned into three-dimensional periodic structures; from Smay *et al.*[34])

Safari and colleagues[5,36,44] pioneered the FDC, in which the stiffness of the filamentary feedstock as well as the viscosity of the extruded colloid-filled, molten polymeric ink must be well controlled. In the molten state, these inks must possess both a low viscosity and a high solids loading to minimize component shrinkage during binder removal and sintering. Similar to injection molding,[44] the ceramic particles must be well dispersed within the polymer to achieve these requirements. As a result of their high colloid volume fraction (~0.5–0.55), molten FDC inks exhibit strong shear thinning behavior (see Fig. 8). Upon deposition, these filaments solidify first at their outer surface, and then radially through their core—exactly opposite of the solidification profile observed for colloidal gel-based inks used in robocasting.

Numerous inks have been formulated for FDC including those based on structural, biomedical, and electrical ceramics.[4,5,36,37] The filled polymer filaments have the advantage of a long shelf-life after initial forming. Melt temperature and extrusion rate (write speed) must be coordinated to match the specific cooling kinetics of a given ink. Fugitive support materials, e.g., unfilled wax filament or water-soluble material developed for fused deposition modeling, are readily available. A key disadvantage of the FDC approach is significant binder content in printed structures, which necessitates a lengthy binder removal procedure. It has recently been reported that the burnout cycle may take several days and can lead to structural defects such as slumping or blistering due to melting of the thermoplastic polymers.[5]

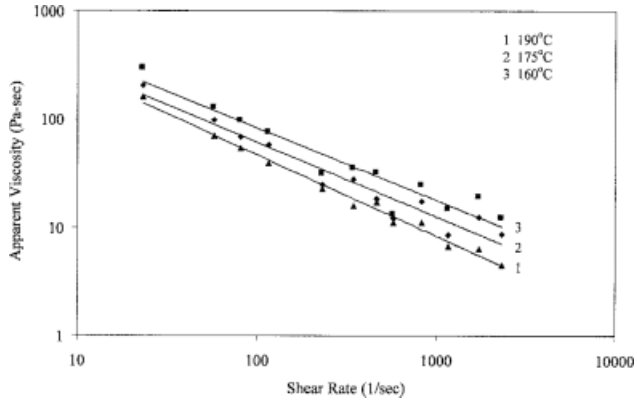

Fig. 8. Apparent viscosity as a function of shear rate for a lead zirconate titanate ink formulated for fused deposition of ceramics heated to varying temperatures (from McNulty[44]).

(3) Potential Shapes

In filament-based DIW, the ink is deposited as a continuous filament. Hence, the interruption of ink flow during assembly is not desirable, so calculations of area filling patterns (tool paths) that minimize the number of start–stop events are useful. Two strategies are used: (1) direction-parallel (or raster) filling and (2) contour-offset filling, as illustrated in Figs 2(c) and (d), respectively. Optimized computational algorithms for each of these tool-path calculations have been described in the literature for milling processes.[62] In both cases, the spacing between adjacent lines is chosen by the user, most often set to be equivalent to the width of the extruded ink filament.

Coordinated three-axis motion is achieved by outputting the calculated tool path to a computer numerical control (CNC) controller. The CNC controller also controls the plunger motion of syringe pumps holding the ink such that volumetric flow rate is tied to position in the tool path. The tool-path calculations yield either raster or contour-offset fill patterns. In either case, filament-based printing faces at least three problems. First, when building solid objects, the ink delivery system must precisely deliver the proper volume of material to fill perfectly the space between adjacent tool-path lines. The tool-path lines represent the locus of points traced by the centerline of the deposition nozzle, but the extruded filament has a finite diameter (assuming that the orifice is circular). The required volumetric flow rate required for filling space is given by

$$Q = h \cdot RW \cdot \mathrm{v} \tag{9}$$

where RW is the road width (distance between adjacent tool path lines). For example, if RW is set equal to the deposition nozzle diameter (d) and $Q = (\pi d^2/4)\mathrm{v}$, the layer thickness must be $h = \pi d/4$. The selection of which variables to fix is a matter of user preference and ink behavior. As the extrusion nozzle is nearly always circular in cross section, the filament must deform upon extrusion to fill the space traced by the nozzle.

The second challenge faced when using a raster or contour tool path is the inevitable need to stop the ink flow, reposition the nozzle on a new tool path, reinitiate the flow, and continue printing. For filament-based printing, it is desirable to minimize the number of start–stop events. Algorithms have been proposed to minimize either the number of start–stop events or the

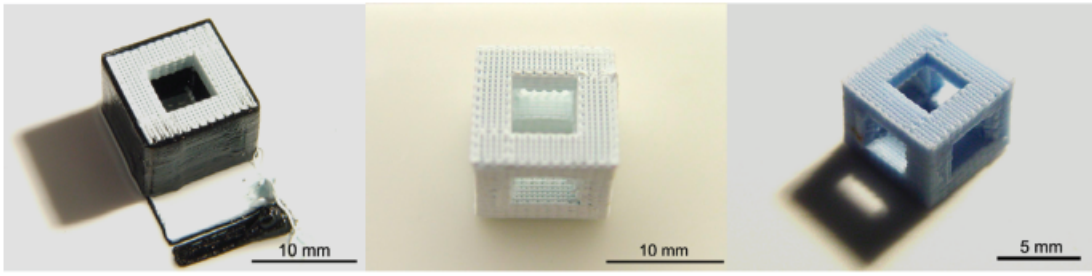

Fig. 9. Open cubic structure assembled by robocasting a concentrated hydroxyapatite ink and a carbon black ink as a fugitive support: (a) as-printed, (b) bisque-fired structure, and (c) sintered ceramic (from Xu and Smay[64]).

distance between the start and stop positions when changing tool-path lines.[63] Figure 2(c) is generated based on the latter algorithm. A corollary to the first and second challenges to layer filling is the potential for underfilling at locations with small radii of curvature along the tool path (e.g., at the hairpin turns in the raster pattern) or where curved paths must be approximated with straight segments such as near the interior holes in the raster pattern. Intelligent algorithms are still under development for these calculations[63] that should enable local variations in flow rate during the writing process.

The third challenge of tool-path calculation involves consideration of the stacking of layers when spanning, cantilevered, or floating elements exist. Algorithms for calculating unsupported regions of the pattern are required along with a suitable fugitive ink. FDC utilizes a second deposition nozzle to print an unfilled wax or water-soluble support material. In the case of printing colloidal fluids or gels, a suitable support should print, solidify, and be chemically compatible with the colloidal ink. Recently, a concentrated ($\phi \approx 0.48$) aqueous gel of carbon black nanoparticles was used as a support material to assemble structures containing both cantilevered elements comprised of a spanning lattice.[64] Figures 9(a)–(c) illustrates green, bisque-fired, and sintered HA hollow cubes, respectively. In Fig. 9(b), the carbon black support has been removed without deformation of the ceramic structure.

High aspect ratio wall and spanning lattice structures assembled from the piezoelectric ceramic $Pb(Zr_{0.53}Ti_{0.47})O_3$ illustrate the similar capabilities of robocasting and FDC (see Fig. 10).

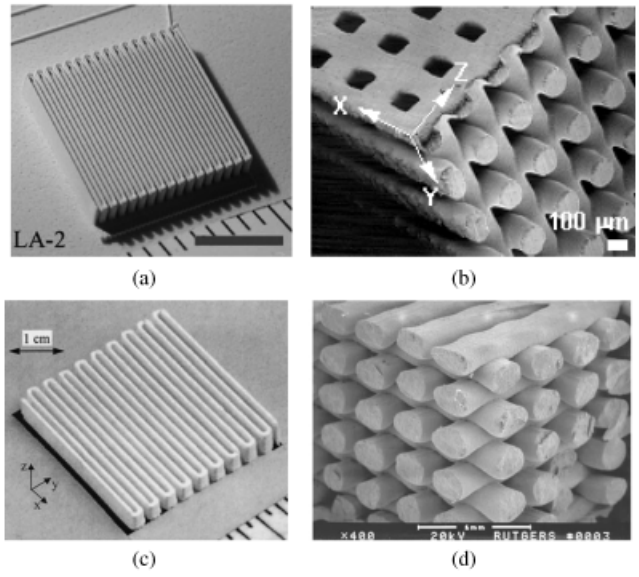

Fig. 10. Piezoelectric ceramic structures formed by robocasting a concentrated lead zirconate titanate ink: (a) high aspect ratio walls (green, scale bar = 5 mm)[65] and (b) spanning lattice structure (sintered) formed by robocasting.[65] (c) high aspect ratio[45] and (d) spanning lattice structures[36] (green) formed by fused deposition of ceramics.

These structures serve as the ceramic skeletons for 2–2 and 3–3 PZT-polymer composites, which are known to display high piezoelectric coefficients and low acoustic impedance, making them attractive for modern sonar and ultrasound systems.[5,6] In both techniques, high aspect ratio and lattice structures are created without the need for support structures. Spanning structures require a solidification time comparable with the time required to traverse the gap in underlying layers. For gel-based inks, the solidification time is of the order of 1 s such that structures with appreciable spanning features may be printed at a high speed ($\sim$1 cm/s), whereas FDC requires longer to solidify (especially as filament size increases), thereby reducing the printing speed or span distance.

(4) Post-Deposition Processing

Analogous to droplet-based DIW techniques, ceramic green bodies produced via filamentary DIW contain varying amounts of binder and can be sintered to a high density (>97% of theoretical). Robocasting of concentrated gel-based inks yields ceramic green bodies with minimal binder ($\sim$2–3 v/o). While their green strength is lower than that of FDC, it may be improved by chemically cross-linking the polymeric species.[42] An important advantage of this route is that binder removal is rather straightforward, with typical debinding schedules of only a few hours required. In sharp contrast, FDC relies on a polymer-rich ink that must be carefully removed on subsequent heat treatment. The binder removal issues are similar to that for wax-based droplet DIW (and injection molding) in that debinding times of several days are often required and component slumping may occur.

Despite the promise of near-net shape fabrication, some applications require precise geometric tolerances that may not be achieved solely through DIW. In these cases, it is advantageous to subsequently machine either the green- or bisque-fired ceramic component via CNC milling. As one example, HA scaffolds of controlled filament size, spacing, and porosity have

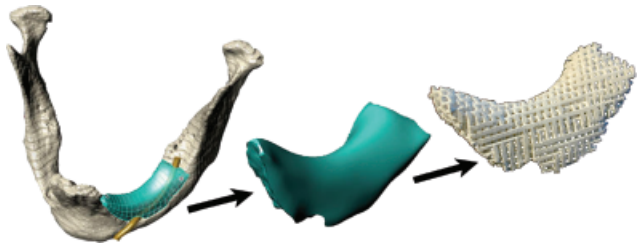

Fig. 11. Image sequence representing the processing steps required to customize a hydroxyapatite (HA) scaffold that fits into a damaged site in a patient mandible (jaw bone): (left) three-dimensional (3D) rendered image compiled from a computed tomography scan of the severely deteriorated mandible shown along with the desired anatomy of the mandible, (center) an isolated view of the solid 3D model defining the desired implant shape, and (right) an optical image of a periodic HA structure produced by robocasting that has been machined into a porous bone scaffold.[66]

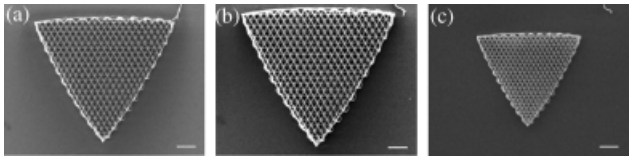

Fig. 12. Scanning electron microscope images of triangular-shaped scaffolds created by a novel filamentary-based writing approach showing their structural evolution: (a) as-patterned, polyamine-rich scaffold, (b) partially cross-linked scaffold after biomimetic silicification, and (c) silica scaffold after heating to 1000°C (all scale bars 20 μm).[70]

shown great promise for bone repair.[66,67] Cesarano *et al.*[66] have shown that robocast scaffolds can be further machined into a customized implant that fits into an individual's unique defect following the methodology shown in Fig. 11. The defective region is first mapped using computed tomography (CT), and these data are then used to manufacture a customized implant before surgery. This final shaping of the 3D scaffold is required because the dimensional tolerance necessary for a well-fitting implant is less than the diameter of the individual HA filaments.

V. Opportunities and Challenges

Looking toward the future, there are many opportunities and challenges for direct ink writing of 3D ceramics via droplet and filamentary approaches. Further advances will require new ink designs,[68,69] better modeling of ink dynamics during deposition, and enhanced robotic and control systems to allow 3D patterning with microscale resolution. As one example, Lewis and colleagues[69,71] recently developed a novel approach for templating 3D ceramic structures with submicron features that combines direct ink writing of a polyamine-rich scaffold with biomimetic silicification (see Fig. 12). This approach circumvents issues related to jamming of ceramic particles during deposition by eliminating them from the ink formulation.

The featured DIW techniques have the capability for multimaterial deposition,[30,70] allowing the creation of advanced composites with locally controlled composition and structure as well as combinatorial studies to be undertaken. However, issues related to efficient micro-mixing and control remain a challenge. Finally, if 3D direct ink writing approaches are to move from prototyping to large-scale production, implementing multiple print heads is needed. This concept is being pursued in two-dimensional writing techniques, such as dip-pen nanolithography,[72] to allow the simultaneous creation of several patterned structures from a single printing platform. Together, these advances will enable the next generation of designer 3D ceramics to be produced for structural, functional, and biological applications.

References

[1]J. A. Lewis, "Colloidal Processing of Ceramics," *J. Am. Ceram. Soc.*, **83**, 2341–59 (2000).
[2]J. A. Lewis and G. M. Gratson, "Direct Writing in Three Dimensions," *Mater. Today*, **7**, 32–39 (2004).
[3]V. Tohver, J. E. Smay, A. Braem, P. V. Braun, and J. A. Lewis, "Nanoparticle Halos. A New Colloid Stabilization Mechanism," *Proc. Nat. Acad. Sci. USA*, **98**, 8950–4 (2001).
[4]M. Allahverdi, S. C. Danforth, M. Jafari, and A. Safari, "Processing of Advanced Electroceramic Components by Fused Deposition Technique," *J. Eur. Ceram. Soc.*, **21**, 1485–90 (2001).
[5]A. Safari and E. K. Akdogan, "Rapid Prototyping of Novel Piezoelectric Composites," *Ferroelectrics*, **331**, 153–79 (2006).
[6]J. E. Smay, J. Cesarano III, B. A. Tuttle, and J. A. Lewis, "Piezoelectric Properties of 3-X Periodic $Pb(Zr_xTi_{1-x})O_3$-Polymer Composites," *J. Appl. Phys.*, **92**, 6119–27 (2002).
[7]J. F. Tressler, S. Alkpu, A. Dogan, and R. E. Newnham, "Functional Composites for Sensors, Actuators and Transducers," *Composites Part A (Appl. Sci. Manuf.)*, **30A**, 477–82 (1999).
[8]P. Calvert, J. Cesarano, H. Chandra, H. Denham, S. Kasichainula, and R. Vaidyanathan, "Toughness in Synthetic and Biological Multilayered Systems," *Philos. Trans. R. Soc. Lond. A*, **360**, 199–202 (2002).
[9]C. S. Marchi, M. Kouzeli, R. Rao, J. A. Lewis, and D. C. Dunand, "Alumina-Aluminum Interpenetrating-Phase Composites with Three-Dimensional Periodic Architecture," *Scripta Mater.*, **49**, 861–6 (2003).
[10]M. P. Rao, A. J. Sanchez-Herencia, G. E. Beltz, R. M. McMeeking, and F. F. Lange, "Laminar Ceramics That Exhibit a Threshold Strength," *Science*, **286**, 102–5 (1999).
[11]R. Soundararajan, G. Kuhn, R. Atisivan, S. Bose, and A. Bandyopadhyay, "Processing of Mullite-Aluminum Composites," *J. Am. Ceram. Soc.*, **84**, 509–13 (2001).
[12]T. M. Chu, J. W. Halloran, S. J. Hollister, and S. E. Feinberg, "Hydroxyapatite Implants with Designed Internal Architecture," *J. Mater. Sci.: Mater. Med.*, **12**, 471–8 (2001).
[13]J. G. Dellinger, J. A. C. Eurell, and R. D. Jamison, "Bone Response to 3D Periodic Hydroxyapatite Scaffolds With and Without Tailored Microporosity to Deliver Morphogenetic Protein," *J. Biomed. Mater. Res. Part A.*, **76A**, 366–76 (2006).
[14]S. Michna, W. Wu, and J. A. Lewis, "Concentrated Hydroxyapatite Inks for Direct-Write Assembly of 3-D Periodic Scaffolds," *Biomaterials*, **26**, 5632–9 (2005).
[15]J. D. Joannopoulos, P. R. Villeneuve, and S. Fan, "Photonic Crystals: Putting a New Twist on Light," *Nature*, **386**, 143–9 (1997).
[16]W. Lee, A. Chan, M. A. Bevan, J. A. Lewis, and P. V. Braun, "Nanoparticle-Mediated Epitaxial Assembly of Colloidal Crystals on Patterned Substrates," *Langmuir*, **20**, 5262–70 (2004).
[17]Y. A. Vlasov, X. A. Bo, J. C. Sturm, and D. J. Norris, "On-Chip Natural Assembly of Silicon Photonic Band Gap Crystals," *Nature*, **414**, 289–93 (2001).
[18]D. B. Chrisey, "The Power of Direct Writing," *Science*, **289**, 879–81 (2000).
[19]E. Sachs, M. Cima, P. Williams, D. Brancazio, and J. Cornie, "3-Dimensional Printing—Rapid Tooling and Prototypes Directly from a Cad Model," *J. Eng. Ind.—Trans. ASME*, **114**, 481–8 (1992).
[20]J. Moon, J. E. Grau, V. Knezevic, M. J. Cima, and E. M. Sachs, "Ink-Jet Printing of Binders for Ceramic Components," *J. Am. Ceram. Soc.*, **85**, 755–62 (2002).
[21]E. Sachs, M. Cima, J. Bredt, A. Curodeau, T. Fan, and D. Brancazio, "CAD-Casting: Direct Fabrication of Ceramic Shells and Cores by Three Dimensional Printing," *Manuf. Rev.*, **5**, 117–26 (1992).
[22]X. Zhao, J. R. G. Evans, and M. J. Edirisinghe, "Direct Ink-Jet Printing of Vertical Walls," *J. Am. Ceram. Soc.*, **85**, 2113–5 (2002).
[23]J. H. Song, M. J. Edirisinghe, and J. R. G. Evans, "Formulation and Multilayer Jet Printing of Ceramic Inks," *J. Am. Ceram. Soc.*, **82**, 3374–80 (1999).
[24]W. D. Teng, M. J. Edirisinghe, and J. R. G. Evans, "Optimization of Dispersion and Viscosity of a Ceramic Jet Printing Ink," *J. Am. Ceram. Soc.*, **80**, 486–94 (1997).
[25]N. Reis, C. Ainsley, and B. Derby, "Viscosity and Acoustic Behavior of Ceramic Suspensions Optimized for Phase-Change Ink-Jet Printing," *J. Am. Ceram. Soc.*, **88**, 802–8 (2005).
[26]T. Wang and B. Derby, "Ink-Jet Printing and Sintering of PZT," *J. Am. Ceram. Soc.*, **88**, 2053–8 (2005).
[27]D. H. Lee and B. Derby, "Preparation of PZT Suspensions for Direct Ink Jet Printing," *J. Eur. Ceram. Soc.*, **24**, 1069–72 (2004).
[28]K. A. M. Seerden, N. Reis, J. R. G. Evans, P. S. Grant, J. W. Halloran, and B. Derby, "Ink-Jet Printing of Wax-Based Alumina Suspensions," *J. Am. Ceram. Soc.*, **84**, 2514–20 (2001).
[29]J. Cesarano III, "A Review of Robocasting Technology"; *Presented at Symposium on Solid Freeform and Additive Fabrication*, Boston, MA, 1999.
[30]J. Cesarano III, T. A. Baer, and P. Calvert, "Recent Developments in Freeform Fabrication of Dense Ceramics from Slurry Deposition"; *Presented at 8th Solid Freeform Fabrication (SFF) Symposium*, University of Texas, Austin, TX, 1997.
[31]J. Cesarano III and P. Calvert, "Freeforming Objects with Low-Binder Slurry"; USA, 2000.
[32]J. Cesarano III, R. Segalman, and P. Calvert, "Robocasting Provides Moldless Fabrication from Slurry Deposition," *Ceram. Ind.*, **148**, 94–102 (1998).
[33]J. E. Smay, J. Cesarano III, and J. A. Lewis, "Colloidal Inks for Directed Assembly of 3-D Periodic Structures," *Langmuir*, **18**, 5429–37 (2002).
[34]J. E. Smay, G. Gratson, R. F. Shepard, J. Cesarano III, and J. A. Lewis, "Directed Colloidal Assembly of 3D Periodic Structures," *Adv. Mater.*, **14**, 1279–83 (2002).
[35]B. A. Tuttle, J. E. Smay, J. Cesarano III, J. A. Voigt, T. W. Scofield, W. R. Olson, and J. A. Lewis, "Robocast $Pb(Zr_{0.95}Ti_{0.05})O_3$ Ceramic Monoliths and Composites," *J. Am. Ceram. Soc.*, **84**, 872–4 (2001).
[36]M. Agarwala, A. Bandyopadhyay, R. van Weewn, A. Safari, S. C. Danforth, N. A. Langrana, V. R. Jamalabad, and P. J. Whalen, "FDC, Rapid Fabrication of Structural Components," *Am. Ceram. Soc. Bull.*, **75**, 60–66 (1996).
[37]S. Rangarajan, G. Qi, N. Venkataraman, A. Safari, and S. C. Danforth, "Powder Processing, Rheology, and Mechanical Properties of Feedstock for Fused Deposition of Si_3N_4 Ceramics," *J. Am. Ceram. Soc.*, **83**, 1663–9 (2000).
[38]S. L. Morissette, J. A. Lewis, P. G. Clem, J. Cesarano III, and D. B. Dimos, "Direct-Write Fabrication of $Pb(Nb,Zr,Ti)O_3$ Devices: Influence of Paste Rheology on Print Morphology and Component Properties," *J. Am. Ceram. Soc.*, **84**, 2462–8 (2001).
[39]W. D. Teng and M. J. Edirisinghe, "Development of Ceramic Inks for Direct Continuous Jet Printing," *J. Am. Ceram. Soc.*, **81**, 1033–6 (1998).
[40]A. R. Bhatti, M. Mott, J. R. G. Evans, and M. J. Edirisinghe, "PZT Pillars for 1–3 Composites Prepared by Ink-Jet Printing," *J. Mater. Sci. Lett.*, **20**, 1245–8 (2001).

[41]J. N. Stuecker, J. Cesarano III, and D. A. Hirschfeld, "Control of the Viscous Behavior of Highly Concentrated Mullite Suspensions for Robocasting," *J. Mat. Proc. Technol.*, **142**, 318–25 (2003).
[42]S. L. Morissette, J. A. Lewis, J. Cesarano III, D. B. Dimos, and T. Baer, "Solid Freeform Fabrication of Aqueous Alumina–Poly(Vinyl Alcohol) Gelcasting Suspensions," *J. Am. Ceram. Soc.*, **83**, 2409–16 (2000).
[43]Q. Li and J. A. Lewis, "Nanoparticle Inks for Directed Assembly of Three-Dimensional Periodic Structures," *Adv. Mater.*, **15**, 1639–43 (2003).
[44]T. F. McNulty, D. J. Shanefield, S. C. Danforth, and A. Safari, "Dispersion of Lead Zirconate Titanate for Fused Deposition of Ceramics," *J. Am. Ceram. Soc.*, **82**, 1757–60 (1999).
[45]G. M. Lous, I. A. Cornejo, T. F. McNulty, A. Safari, and S. C. Danforth, "Fabrication of Piezoelectric Ceramic/Polymer Composite Transducers Using Fused Deposition of Ceramics," *J. Am. Ceram. Soc.*, **83**, 124–8 (2000).
[46]3D Systems Inc. *StereoLithography Interface Specification*. 3D Systems Inc., Valencia, Company literature, October 1989.
[47]J. N. Stuecker, "Freeform Fabrication and Near Net Shape Processing of Composites from Mullite and Kaolin Ceramics"; M.S. Thesis, New Mexico Institute of Mining and Technology, Socorro, NM, 1999.
[48]M. Greul, F. Petzoldt, and M. Greulich, "Rapid Prototyping of Powder Binder Mixtures Using the Multiphase Jet Solidification (MJS) Process," *Adv. Powder Metall. Particulate Mater.*, **3**, 18/153–9 (1997).
[49]R. Vaidyanathan, J. Walish, J. L. Lombardi, S. Kasichainula, P. Calvert, and K. C. Cooper, "The Extrusion Freeforming of Functional Ceramic Prototypes," *J. Minerals Metals. Mater. Soc.*, **52**, 34–7 (2000).
[50]M. Greul, T. Pintat, and M. Greulich, "Rapid Prototyping of Functional Metallic and Ceramic Parts Using the Multiphase Jet Solidification (MJS) Process," *Adv. Powder Metall. Particulate Mater.*, **2**, 7/281–7 (1996).
[51]R. Lenk, "Rapid Prototyping of Ceramic Components," *Adv. Eng. Mater.*, **2**, 40–47 (2000).
[52]R. Buscall, J. I. McGowan, and A. J. Morton-Jones, "The Rheology of Concentrated Dispersions of Weakly Attracting Colloidal Particles with and without Wall Slip," *J. Rheol.*, **37**, 621–41 (1993).
[53]W. H. Herschel and R. Bulkley, "Konsistenzmessungen von Gummi-Benzollosungen," *Kolloid Z.*, **39**, 291 (1926).
[54]D. M. Kalyon, P. Yaras, B. Aral, and U. Yilmazer, "Rheological Behavior of a Concentrated Suspension: A Solid Rocket Fuel Simulant," *J. Rheol.*, **37**, 35–53 (1993).
[55]R. J. Hunter, *Foundations of Colloid Science*, Vol. 1. Oxford University Press Inc., New York, 1992.
[56]S. Nadkarni and J. E. Smay, "Concentrated Barium Titanate Colloidal Gels Prepared by Bridging Flocculation for Use in Solid Freeform Fabrication," *J. Am. Ceram. Soc.*, **89**, 96–103 (2006).
[57]G. M. Channell, K. T. Miller, and C. F. Zukoski, "Effects of Microstructure on the Compressive Yield Stress," *A.I.Ch.E. J.*, **46**, 72–78 (2000).
[58]R. B. Rao, K. L. Krafcik, A. M. Morales, and J. A. Lewis, "Microfabricated Deposition Nozzles for Direct-Write Assembly of Three-Dimensional Periodic Structures," *Adv. Mater.*, **17**, 289–93 (2005).
[59]E. L. Corral, J. Cesarano, J. N. Stuecker, and E. V. Barrera, "Processing of Carbon Nanofiber Reinforced Silicon Nitride Matrix Composites"; *Presented at Symposium on Rapid Prototyping of Materials*, Columbus, OH, 2002.
[60]G. He, D. A. Hirschfeld, and J. Cesarano III, "Processing and Mechanical Properties of Si_3N_4 Formed by Robocasting Aqueous Slurries"; *Presented at 24th International Conference & Exposition on Engineering Ceramics and Structures*, Cocoa Beach, FL, 2000.
[61]G. He, D. A. Hirschfeld, J. Cesarano III, and J. N. Stuecker, "Processing of Silicon Nitride–Tungsten Prototypes"; pp. 325–3 in *Ceramics Transactions, Vol. 114 Functionally Graded Materials 2000*, Edited by K. Trumble, K. Bowman, I. Remanis, and S. Sampath. American Ceramic Society, Westerville, OH, 2001.
[62]M. Held, *On the Computational Geometry of Pocket Machining*. Springer-Verlag, Berlin, 1991.
[63]D. Qiu, N. A. Langrana, S. C. Danforth, A. Safari, and M. Fafari, "Intelligent Toolpath for Extrusion-Based LM Processes," *Rapid Prototyping J.*, **7**, 18–23 (2001).
[64]J. Xu and J. E. Smay, "Concentrated, Aqueous Carbon Black Colloidal Gel Ink for Support Structures in Solid Freeform Fabrication," *J. Am. Ceram. Soc.*, (2006), in preparation.
[65]J. E. Smay, "Directed Colloidal Assembly and Characterization of PZT-Polymer Composites"; M.S. Thesis, University of Illinois, Urbana-Champaign.
[66]J. Cesarano III, J. G. Dellinger, M. P. Saavedra, D. D. Gill, R. D. Jamison, B. A. Grosser, J. M. Sinn-Hanlon, and M. S. Goldwasser, "Customization of Load-Bearing Hydroxyapatite Lattice Scaffolds," *Int. J. Appl. Ceram. Technol.*, **2**, 212–20 (2005).
[67]J. G. Dellinger, "Development of Model Hydroxyapatite Bone Scaffolds with Multiscale Porosity for Potential Load Bearing Applications"; M.S. Thesis, University of Illinois, Urbana-Champaign, 2005.
[68]H. Y. Fan, Y. F. Lu, A. Stump, S. T. Reed, T. Baer, R. Schunk, V. Perez-Luna, G. P. Lopez, and C. J. Brinker, "Rapid Prototyping of Patterned Functional Nanostructures," *Nature*, **405**, 56–60 (2000).
[69]G. Gratson, M. Xu, and J. A. Lewis, "Direct Writing of Three Dimensional Webs," *Nature*, **428**, 386 (2004).
[70]J. A. Lewis, "Direct-Write Assembly of Ceramics from Colloidal Inks," *Curr. Opin. Solid State Mater. Sci.*, **6**, 245–50 (2002).
[71]M. Xu, G. M. Gratson, E. Duoss, R. F. Shepard, and J. A. Lewis, "Biomimetic Silicification of Polyamine-Rich Scaffolds Assembled by Direct Writing," *Soft Matter*, **2**, 205–9 (2006).
[72]R. D. Piner, J. Zhu, F. Xu, S. Hong, and C. A. Mirkin, "Dip-Pen Nanolithography," *Science*, **29**, 661–3 (1999). □

Dr. Jennifer A. Lewis received a B.S. degree with high honors in ceramic engineering from the University of Illinois at Urbana-Champaign (UIUC) in 1986 followed by a Sc.D. in ceramic science from the Massachusetts Institute of Technology (MIT) in 1991. She joined the faculty of the materials science and engineering department at UIUC in 1990, where she is currently appointed as the Hans Thurnauer Professor of Materials Science and Engineering and the Interim Director of the Frederick Seitz Materials Research Laboratory. She received the NSF Presidential Faculty Fellow Award (1994), the Brunaeur Award from the American Ceramic Society (2003), and was recently named a Fellow of the American Ceramic Society (2005). She is currently an Associate Editor of the *Journal of the American Ceramic Society* and serves on the Editorial Advisory Boards of *Langmuir* and *Soft Matter*. Her research focuses on the directed assembly of functional ceramic, microfluidic, photonic, and tissue engineering structures from colloidal, nanoparticle, and polymeric building blocks. Her work has been featured in *The Economist, The Technology Review, Chemical & Engineering News, Lab on a Chip, The Scientist, Photonics Spectra, and Materials Today*.

Dr. James E. Smay earned a B.S. degree in Mechanical Engineering from Oklahoma State University (OSU) in 1996 and a Ph.D. degree in Materials Science and Engineering from the University of Illinois at Urbana-Champaign (UIUC) in 2002. In 2002, Dr. Smay received the Victor K. LaMer award from the American Chemical Society, in recognition of his Ph.D. research. He joined the Chemical Engineering Department at Oklahoma State University as an Assistant Professor in 2002. Dr. Smay's research intersts lie in the area of novel colloidal processing techniques and application of ceramic, metallic, and polymeric materials in engineering. In 2005, he received the Presidential Early Career Award for Scientists and Engineers (PECASE) following a NSF CAREER award for his work.

Mr. John Stuecker received his B.S. in Materials Science and Engineering at Virginia Tech in 1997 and his M.S. in Materials Engineering at New Mexico Institute of Mining and Technology in 1999. He then joined Sandia National Laboratories, where he is currently a member of the technical staff. His research interests focus on precision robotic writing and aerosol deposition of materials, including composites and fuel cell systems as well as the application of colloidal science to explosives, catalysts, and electronic devices.

Dr. Joseph Cesarano III received his B.S. degree in ceramic engineering from Alfred University in 1983, and his Ph.D. in Materials Science from the University of Washington in 1989. He joined Sandia National Laboratories in Albuquerque, New Mexico in 1989 and is currently a Materials Scientist and Principle Member of the Technical Staff in the Ceramic Materials Department.

His expertise is in the area of colloidal science and manipulation of inter-particle forces for optimization of handling, processing, and manufacturing materials. His research interests focus on the dispersion and processing of highly concentrated fine-particle suspensions, freeform fabrication, near-net-shape processing, and precision conformal printing of materials. He leads multi-disciplinary teams to improve materials processes for manufacturing and development of structures yielding unique performance. He is co-inventor of the robocasting technology and is actively pursuing the utility of lattice structures for catalyst supports, diesel particulate filtration, and artificial bone scaffolds. He has over 30 publications, 4 patents, and four patents pending. His Ph.D. work on polyelectrolyte stabilization has been cited over 570 times.